Hydrogen storage properties of 2 Mg–Fe mixtures processed by hot extrusion: Effect of ram speeds

Gisele Ferreira de Lima Andreani, Maria Regina Martins Triques, Daniel Rodrigo Leiva, Virginie Roche, Kátia Regina Cardoso, Tomaz Toshimi Ishikawa, Walter Jose Botta, Alberto Moreira Jorge

Hydrogen Storage Properties of 2Mg-Fe Mixtures Processed by Hot Extrusion: Effect of Ram Speeds

Gisele Ferreira de Lima Andreani[1], Maria Regina Martins Triques[2], Daniel Rodrigo Leiva[2], Virginie Roche[3], Kátia Regina Cardoso[1,4], Tomaz Toshimi Ishikawa[2], Walter José Botta [2], Alberto Moreira Jorge Jr[2,3,4]

[1]Science and Technology Institute, Federal University of São Paulo, São José dos Campos-SP, Brazil

[2]Department of Materials Engineering, Federal University of São Carlos, São Carlos – SP, Brazil

[3]Grenoble Alpes University, CNRS, LEPMI, F-38000 Grenoble, France

[4]Grenoble Alpes University, CNRS, SIMAP, F-38000 Grenoble, France

*corresponding author: moreira@ufscar.br, Jorge.Moreira@lepmi.grenoble-inp.fr

Abstract

Hot extrusion processing was used for producing bulk samples of 2MgFe mixtures adequate to hydrogen storage. High-energy ball milling was used to prepare 2MgFe powder mixtures, which were cold-pressed into cylindrical pre-forms. Such pre-forms were then processed by hot extrusion (at 300 ^{o}C and extrusion ratio of 3/1) to produce bulk samples. In this work, it was analyzed the influence of the ram speed (1, 5, and 10 mm/min) on the microstructure and hydrogen sorption properties of obtained bulks. Nanograins, which resulted from the milling process, remained in the nanosize after hot extrusion conditions. More porous samples were produced at a ram speed of 1 mm/min, which also kept the

smaller grain size. These features led the sample processed at 1 mm/min to absorb about 4.8 wt% of H, which was higher than precursor powders that absorbed around 4.3 wt% of H. This behavior was assigned to a redistribution of Fe during extrusion, which was kept agglomerated in the powders. The results also showed that desorption temperatures of bulks were very similar to that of 2MgFe powders. Such behavior is very interesting, considering the lower surface area of bulks. When compared to MgH_2 powders, samples processed in this work presented much lower desorption temperatures. Except for the sample processed at 10 mm/min, all other samples fully desorbed in less than 8 min at 350 ^{o}C, while commercial MgH2 would take much more than 40 min for complete desorption.

Key-words: hydrogen storage, Mg hydrides, hot-extrusion, complex hydrides

Introduction

Since the 1990s, the scientific community has been interested in the development of a hydrogen economy based on such gas as an energy carrier [1-3]. Mg and Mg-based composites are attractive materials for hydrogen storage. The high hydrogen mass capacity of MgH_2 (7.6 wt.%) and Mg_2FeH_6 (5.5 wt.%), their reversibility, and low cost make them promising for energy storage applications [1, 3]. However, the high stability (desorption temperatures), the slow H-sorption kinetics and the weak resistance to air contaminants, which quickly degrade the H-sorption properties, limit the practical application of these hydrides [1].

It is known that nanostructured hydrogen storage materials produced by high-energy ball milling (HEBM) or mechanical alloying (MA) present better hydrogen sorption kinetics. The increased surface area and the structural defects, created by those processing routes, lower the activation energy barriers [2, 4-6]. With additions of catalysts, it is possible to produce a synergic effect between surface area, structural defects, and catalyst effect [7-31], thus further improving hydrogenation properties. Addition of Fe as a catalyst can decrease the decomposition temperature of MgH_2 by more than 100 ^{o}C, by reducing the activation energy for hydride decomposition. Additionally, iron can prevent the agglomeration of Mg and also act as Mg_2FeH_6 former [11, 17-19, 23-40]. However, there are several drawbacks in using powders for hydrogen storage, including the occurrence of surface contamination, the potential fire risk, and health concerns.

As an alternative, powder consolidation methods, including Severe Plastic Deformation (SPD) techniques, cold rolling and extrusion have been recently employed to develop hydrogen storage materials [7-24, 41-75]. In general, these techniques produce a microstructure with a high density of defects (for instance, dislocations) due to a high level of deformation, grain refinement (when starting from bulks) that may lead to nanostructures, and bulks that are safer, easier to manipulate, and more air-resistant than powders.

Lima et al. [47-49] have reported successful results in the production of bulk 2MgFe composites by hot-extrusion, by SPD, and by using a combination of hot-extrusion and SPD processes. By using hot-extrusion, they found excellent hydrogenation properties similar to as acquired with either MA or SPD processes. Such features were attributed to the better air resistance of bulks, the porosity (since powders were consolidated by hot-extrusion), and the pinning effect of Mg

grain boundaries by the Fe particulate, which can keep the nanoscale level during hot working.

In previous works [50-52], we have investigated the influence of the extrusion ratio and temperature used during powder consolidation processing. In such investigations, it was verified that the smaller extrusion ratio [50], the higher the porosity and, consequently, the better the hydrogenation properties. Also, when processing 2Mg-Fe mixtures at 300 °C, the bulk samples presented the best synergetic combination of grain sizes and desirable texture along (002) plan for Mg, thus resulting in fastest kinetic of H-absorption without any incubation time [51, 52].

In this work, results are presented concerning the influence of the ram speed during hot-extrusion of 2Mg-Fe mixtures on the microstructure and its consequence on the hydrogenation properties.

Experimental

Pure powders of Mg (-20+100 mesh, 99.98%, Alfa Aesar) and Fe (-22 mesh, 99.998%, Alfa Aesar) were mixed by high energy ball milling in a stoichiometry 2Mg-Fe (at.%). The milling was performed in a Fritsch P7planetary ball mill under an argon atmosphere, at 600 rpm, using a ball-to-powder ratio of 40:1. Powders were milled for four hours, after which they were sieved in an 80 mesh sieve.

Samples (~1g) from the powder mixture were cold-pressed into pre-forms, which were then hot-extruded in a conventional Universal Testing Machine, EMIC Ltda DL-60.000, using the best conditions established in previous work: extrusion

ratio of 3/1 [50], at an extrusion temperature of 300°C [51, 52]. Ram speeds were 1, 5, and 10 mm/min. Extruded samples were named according to their processing speeds; and so hereafter they will be referred to as V1, V5, and V10, respectively for 1, 5, and 10 mm/min.

Bulk samples were hydrogenated in a Sievert's type apparatus to perform sample activation, to acquire absorption kinetics' curves, and to determine incubation times. For such, the hydrogen pressure was kept at 1.5 MPa for 20 h at the temperature of 400 ºC, aiming to obtain the Mg_2FeH_6 complex hydride with the maximum capacity (5.5% of H_2) and to favor the hydrogenation of such bulk samples. Mg powders were also used for comparison.

Thermal analyzes using differential scanning calorimetry (DSC) and thermogravimetry (TG), were performed in a NETZSCH STA 449C were used to evaluate the thermodynamic stability of hydrides, capacities and desorption kinetics of H_2, which were compared to commercial MgH_2 powders.

The percentage by weight of H_2 was calculated using the procedure suggested by Varin et al. [76], as follows. Assuming the hydrogen as an ideal gas, the Volumetric Method was employed to achieve H_2 wt% applying the following equations [76]:

$$\text{wt.}\,\%\,H_2 = (m_H \times 100)/(m_{Hydride}) \quad \text{Eq (1)}$$

$$m_{Hydride} = m_H + m_s \quad \text{Eq(2)}$$

$$m_H = (2.016 \times \Delta P \times V/(R \times T)) \quad \text{Eq (3)}$$

In Equation (1), wt. % H_2 is the weight percent of molecular hydrogen, m_H is the absorbed hydrogen in molecular mass determined by utilizing the number of gas moles ($\Delta n=((\Delta P \times V)/((R \times T)))$). In Equation (2), m_s is the mass of metal (mass

of 2MgFe mixture). Therefore, m_H + m_s is the mass of hydride ($m_{Hydride}$). In Equation (3), R is the universal gas constant (R = 8.314472 J mol-1 K-1), V (= V_h + V_r) is the total volume, V_r is the calibrated volume at the reservoir temperature, Vh is the calibrated volume of the holder at the furnace temperature, T (K) denotes the H-absorption temperature inside of the furnace, and ΔP is the pressure range of hydrogen gas in the system during hydrogen absorption.

Information regarding the structure and phases' identification after each processing step were obtained by X-ray diffraction (XRD) using monochromatic CuKα radiation with an angular pass of 0.032^o in a Rigaku DMAX diffractometer, in which was used a C-monochromator to avoid fluorescence of Fe. The Rietveld method was employed to refine diffraction patterns using the Maud software [77, 78].

Scanning electron microscopy (SEM) and transmission electron microscopy (TEM) were conducted to characterize the microstructure and morphology of samples using respectively an FEI INSPECT S50 microscope, and an FEI CM-120 microscope operated at 120 kV.

Extruded samples were cut from the cross-section of each billet (perpendicular to the pressing direction) and embedded in resin, after which they were prepared by usual metallographic methods, including multistep grinding employing SiC abrasive paper (320, 400, 600, 800, 1200 and 2000 grit). At the final step of preparation, they were polished utilizing 2500-grit SiC paper and, finally, with 0.02-μm colloidal silica suspension, and diamond polishing paste. Such samples were used to be observed in the SEM using electron backscattered (BSE) mode to emphasize the chemical contrast.

Powders for TEM observations were placed in an ethanol suspension that was ultrasonicated to disperse powder agglomerates. A droplet of this suspension was poured on a 3mm in diameter copper grid coated with carbon film. Thin foil TEM samples were prepared from the cross-section of the as-extruded pieces. Small flat pieces were cut from billets with diamond wheel, being carefully ground up to 50-70 μm thick and punched in 3.0 mm diameter disks with an appropriate device. Finally, thin areas were obtained by ion-milling using a Gatan precision ion polishing system (model 691) with beam energy of 5keV under an argon atmosphere. Both kinds of samples were hydrogenated for TEM observation.

Mg and Mg-based composites and their hydrides are humidity and oxygen-sensitive. However, to ascertain their resistance to such an atmosphere, samples used in this work were stored in the air.

Results and discussions

Figure 1 shows the XRD patterns of the extruded samples (V1, V5, and V10). As expected, only α-Mg and α-Fe phases were indexed in all of them. Broad and low-intensity peaks are observed in all the diffractograms, indicating the presence of refined grains after the extrusions. Table 1 shows the average crystallite sizes estimated by the Rietveld method. In general, one may observe that in all the extruded samples, the crystallites were larger than in the starting powders, which grew with the increase of the ram speed [50-52]. Such an increase of crystallite size indicates that adiabatic heating is taking place during extrusion. When mechanical stress is applied, a considerable amount of mechanical work per unit volume ($\int \sigma d\varepsilon$) is converted into heat. In all the mechanical working operations

there is the occurrence of deformation heating, which increases with the product of stress (σ) and strain (ε), and σ increases with the strain rate (ram speed). As the time of extrusion is inversely proportional to the ram speed, when the ram speed (strain rate) increases, the time to remove heat is reduced, and such conditions approach the adiabatic ones. Therefore, the higher the ram speed, the higher the temperature increase, and the larger the resulting crystallite size.

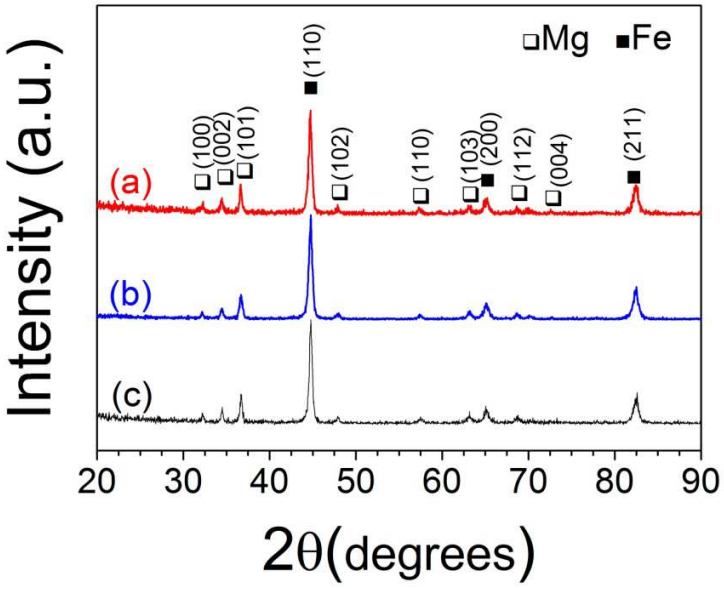

Figure1 – XRD patterns of the mixture of 2Mg-Fe, extruded at 300^{o}C: (a) V1; (b) V5; (c) V10.

Table 1 - Average crystallite size (nm ± 5 nm), estimated by the Rietveld method.

Phase	as-milled [50-52]	V1	V5	V10
Mg	37	43	69	106
Fe	39	41	48	56
Rw/Rexp*	1.03	1.01	1.09	1.09

*Goodness of fitting (GOF= Rw/Rexp), satisfactory ≤ 1.3

Although both Mg and Fe crystallite sizes have increased, Fe crystallites increased less. Iron has to diffuse through moving Mg grain boundaries. Once its diffusion coefficient in Mg is minimal (10^{-16} m^2/s [79]), the growth rate of Fe crystallites is limited. On the other hand, such a very small crystallite size has very high boundary energy, which is beneficial for pinning Mg grain boundaries, thus limiting also their growth.

Figure 2 presents BSE-SEM images of extruded samples in comparison with powders of 2MgFe, being (a) for V1, (b) for V5 and (c) for V10, respectively for the extruded conditions, and (d) for powders. As it may be seen, despite agglomeration, iron was well redistributed along with extruded samples. However, in the case of powders, there are large areas without the presence of iron, indicating that it has agglomerated preferentially in some regions. It is also noteworthy that samples' densification increases with the ram speed, i.e., the higher the ram speed, the lower the porosity present in the samples.

Figure 3 shows curves of the first hydrogen absorption performed in a Sieverts-type apparatus at 400 ^oC under 15 bar of H_2, for samples extruded at different ram speeds compared to starting 2MgFe powders and pure powders of Mg. As one may observe, there is an essential difference in hydrogen capacities. Such capacities decreased in the sequence of V1 (~4.8 wt.%), V5 (~4.4 wt.%), 2MgFe powders (4.3 wt.%), Mg (3,4 wt%), and V10, which had the worst behavior after 20 h of hydrogenation (~2.5 wt.%).

As expected, all extruded samples had slower absorption kinetics than the 2MgFe powders, which can be explained by the differences in surface areas, which

is larger for the powders. However, powders reached saturation after almost 10h, while sample V1 reached it after ~15h. Samples V5 and V10 would take more time to reach their maximum capacity.

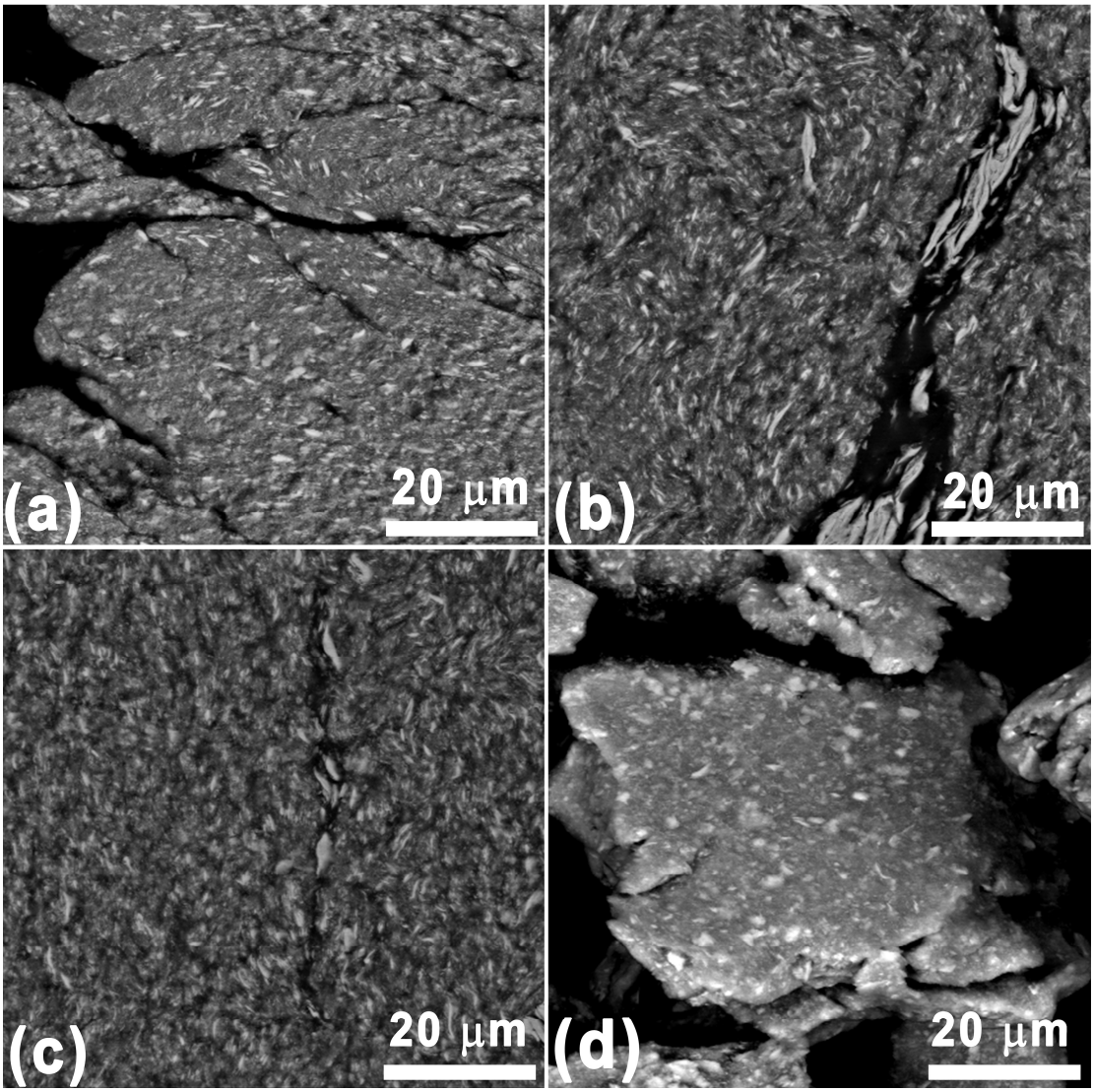

Figure 2 - BSE-SEM images of extruded samples and powders. (a) extruded at V1, (b) extruded at V5, (c) extruded at V10 and (d) powders.

The behavior presented by extruded samples, not excluding the catalytic effect of Fe, is probably due to three crucial factors: (1) smaller surface area

because extruded samples are in the bulk form, (2) lack of porosity that tends to decrease with the increase of ram speed (Fig. 2), and (3) grain size (Table 1). However, one may observe that factors (2) and (3) may be prevailing because kinetics are slowed down, and capacities are decreased following precisely the increasing sequence of ram speeds (decreasing porosity) and the increase of grain sizes, as presented in Figure 2 and Table 1, respectively.

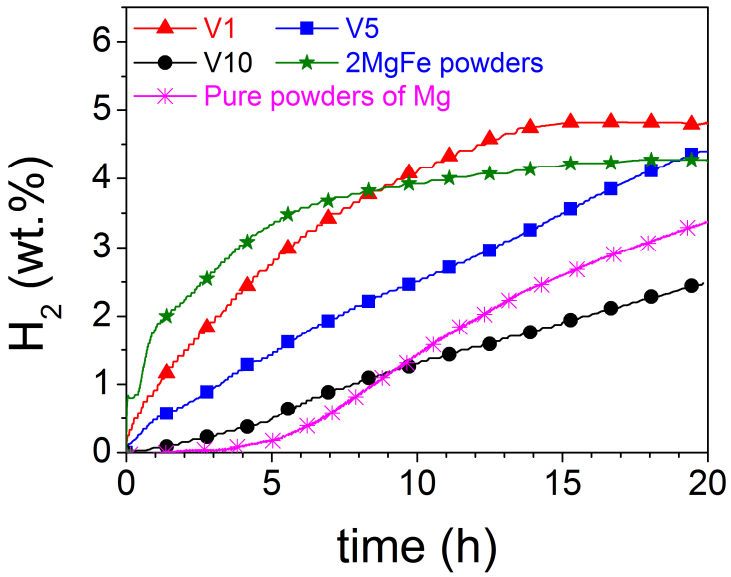

Figure 3 - Curves of the first hydrogen absorption performed in a Sieverts-type apparatus at 400°C under 15 bar H_2, for samples V1, V5, and V10, compared to starting powders of 2MgFe and pure powders of Mg.

However, even explaining the different capacities and kinetics between extruded samples, the above argumentation does not justify why the hydrogen capacity of powders was smaller than for conditions V1 and V5. These results can be better understood by evaluating the XRD patterns for samples after hydrogenation, as shown in Figure 4.

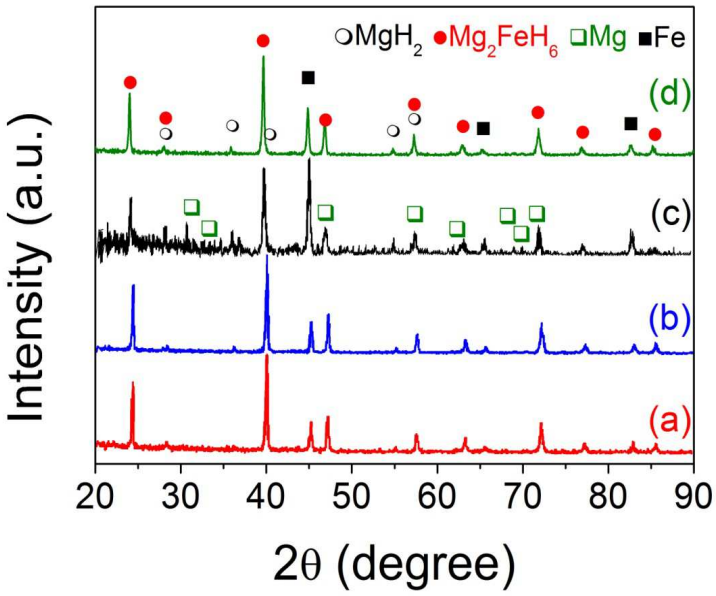

Figure 4 - XRD patterns of hydrogenated powders and extruded samples of 2Mg-Fe: (a) V1, (b) V5, (c) V10, and (d) powders.

Indexing of the Bragg peaks shows that, after hydrogenation, both hydrides, Mg_2FeH_6 (in a more substantial proportion) and MgH_2 were formed. Table 2 shows the relative amounts of MgH_2 and Mg_2FeH_6 obtained by Rietveld refinement of the patterns. The fraction of MgH_2 is smaller in all conditions, but since the relative proportions of the two types of hydrides varies from sample to sample the small differences between the extruded samples and the reference powder can be justified. Bragg peaks relative to residual Fe are also observed in all diffraction patterns, and peaks corresponding to residual Mg were only found in sample V10 and, in a small percentage, in the powders. However, comparing relative amounts of iron between powders and conditions V1 and V5, one may observe that remaining iron in the powders is more significant than in these two other conditions. If one considers that also there was residual Mg in the powders, it is

possible to affirm that the conversion of 2MgFe into Mg_2FeH_6 was smaller in the powders than for conditions V1 and V5. This fact may be explained by the worst distribution of iron in the powders when compared to extruded samples, as seen in Figure 2. In other words, Fe agglomeration in specific regions in the powders hampered the complete transformation, thus reducing the powders' capacity.

Table 2 - Calculated distribution of Mg, Fe, MgH_2, and Mg_2FeH_6 for the various samples using Rietveld refinement.

Condition	Mg (%)	Fe (%)	MgH2 (%)	Mg_2FeH_6 (%)
V1	0	22.25	8.47	69.29
V5	0	23.30	5.92	70.78
V10	17.09	41.31	9.51	32.09
Powders	3.01	29.52	6.02	61.45

However, it is remarkable that none of the conditions completed the conversion to the complex hydride. This fact could also be related to the size and distribution of Fe agglomerates, which, even being better distributed in extruded samples, continued to be agglomerated with large particle sizes in addition to decreased porosity in such samples. As the diffusion of Fe in Mg is very slow at the hydrogenation temperature (the diffusion coefficient at 400 ^oC is about 10^{-18} $m^2.s^{-1}$ [80], probably the conversion was kept around those large particles and in smaller ones as presented in Figure 5.

It is also noteworthy that the maximum capacity, even considering the presence of MgH_2, was only 4.8 wt%, reached by condition V1. It must be borne in mind that the expected capacity for the complex hydride should be 5.5 wt%. The reason for this behavior may be explained by analyzing Equations (1-3) under the light of results presented in Table 2. If one pay attention in Table 2, it will possible, as stated before, to observe that there was no complete conversion of the mixture 2MgFe into Mg_2FeH_6 for all conditions, remaining a considerable and crescent amount of Fe following the sequence of V1, V2, powders and V10, and the presence of Mg in the powders and condition V10. Therefore, one may infer that as Equations (1-3) calculate the H2 wt % considering the total mass and as materials were not totally hydrogenated, the total mass of hydrogen will be decreased.

Contrarily to all other samples, Mg powders were sensible to oxidation and presented an incubation time of about 4 hours. Such oxidation also slowed down its kinetics and decreased its maximum capacity during the hydrogenation, which, after 43 hours, was of only ~5.4 wt%. The absence of incubation time in any other condition than in Mg powders means that oxidation did not affect hydrogenation, probably due to the catalytic effect of iron in 2MgFe samples and reduced surface area in extruded ones.

Figure 5 present bright field images obtained by TEM for hydrogenated 2MgFe powders and V1, V5 and V10 extruded and hydrogenated samples, together with the selected area diffraction patterns in the respective insets. The diffraction patterns indicate that the dimensions of the microstructure remain in the range of nanometers. This fact may be ascribed to the pinning effect of Fe particulate which, as observed in Table 1, continues to be in the scale of a few nanometers. Figure 6 presents the indexation of diffraction patterns shown in the

insets of Figure 5. As one may note, such indexations confirm the presence of all phases indicated in Figure 4. However, the samples were very thin and hydrogenated to be observed in the TEM. Therefore, it would be expected that they would become fully hydrogenated. Nonetheless, one must be borne in mind that the electron beam can start hydrogen desorption from the sample within the microscope and phases such Mg and Fe are also supposed to appear.

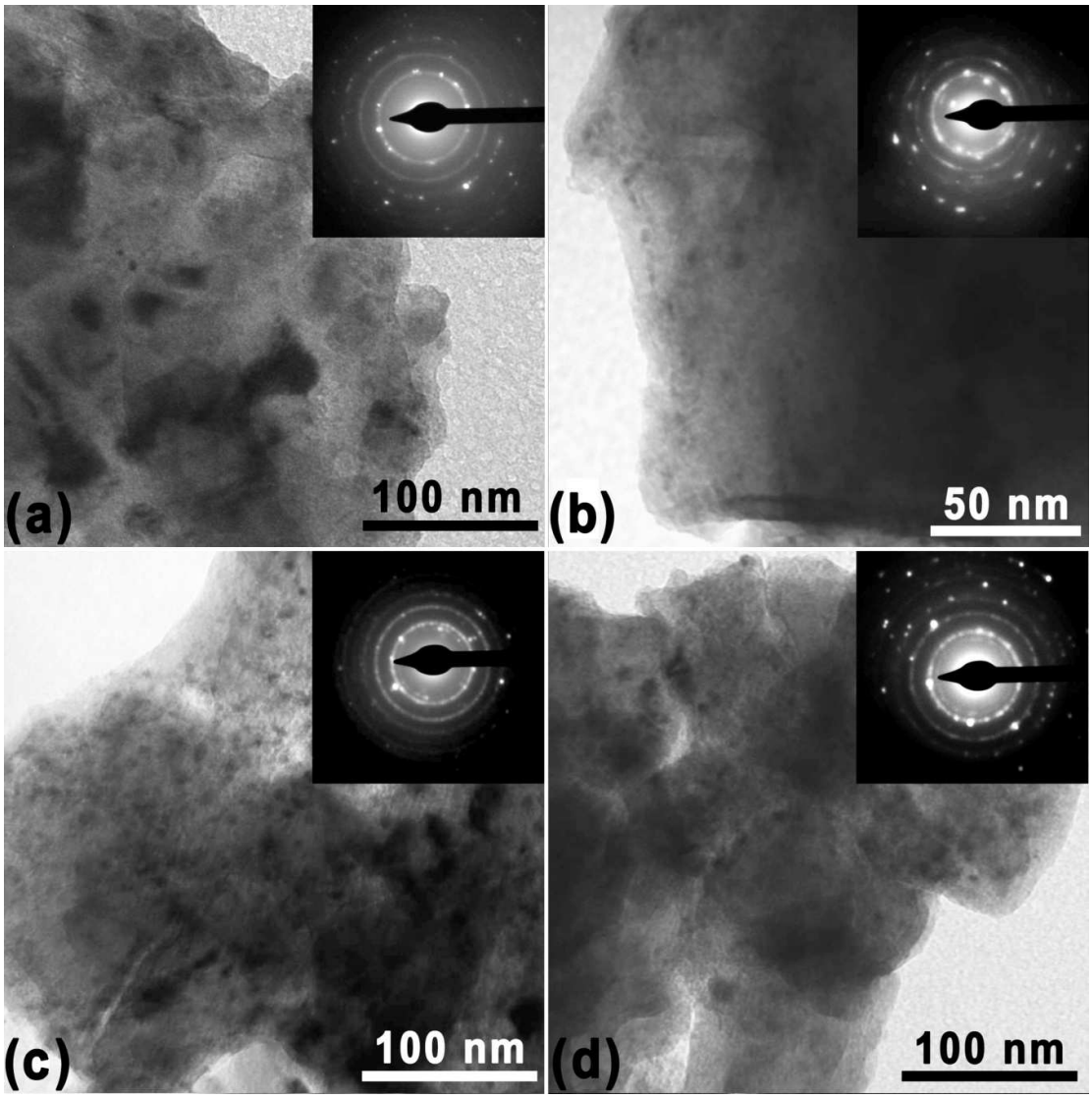

Figure 5 - BF-TEM images of the hydrogenated samples: (a) 2MgFe powder. (b) V1. (c) V5. (d) V10. The insets correspond to their respective selected area electron diffraction patterns (SAEDP).

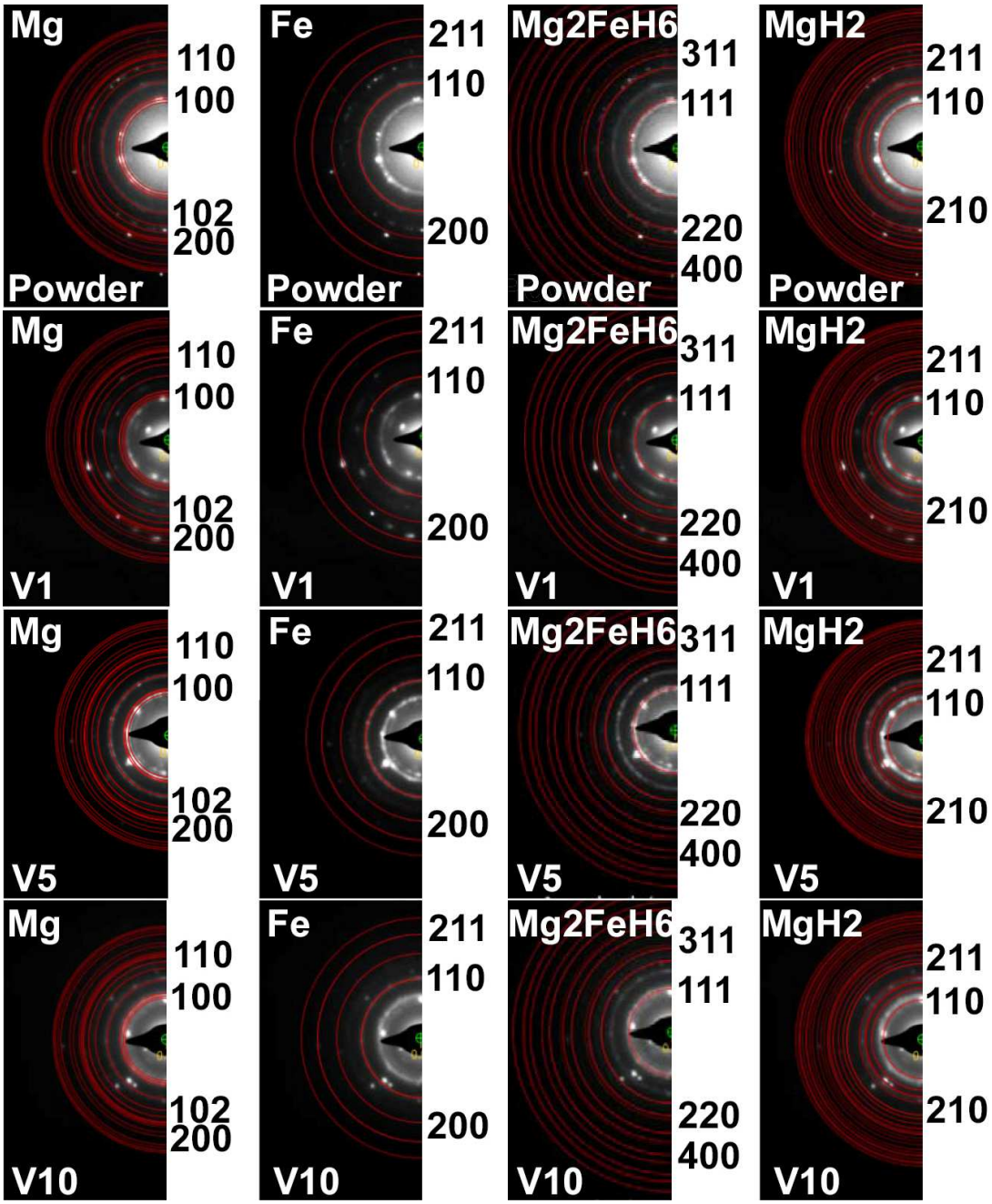

Figure 6 - Indexation of diffraction patterns shown in the insets of Figure 5.

Figure 7a shows DSC results for hydrogenated samples V1, V5, and V10, in comparison with powders of 2MgFe and commercial MgH_2. Firstly, it is evident that hydrogen desorption temperatures in any sample with 2MgFe are lower than those of commercial MgH_2, due to the catalytic effect of Fe. Furthermore, as expected,

the hydrogen onset (260 ^{o}C) and desorption peak temperatures (315 ^{o}C) were lower for the 2MgFe powder mixture than for the bulks of the extruded samples. For extruded samples, these temperatures were very close to each other. However, they were smaller and the same for V1 and V5, 270 ^{o}C (onset) and 326 ^{o}C (desorption peak). From these observations, it is clear that Fe has a strong kinetic effect in the desorption of the hydrides present. However, the general unanimity is that the Mg_2FeH_6 stability does not vary markedly from that of β-MgH_2 (−74.4 kJ mol^{-1} H_2 [81]).

By analyzing the TG data (Fig. 7b), one may observe that the starting desorption temperatures follow the same behavior seen in the DSC curves of Figure 7a. Also, the desorbed mass follows the same behavior of the absorption as shown in Figure 3, i.e., very close to each other, but decreasing following the ram speed sequence of V1, V5, powders, and V10.

The kinetics of hydrogen desorption, shown in Figure 7c, was faster for powders and almost the same for samples V1 and V5. Sample V10 had the worst behavior. Powders and samples V1 and V5 fully desorbed in less than 8 min, while commercial MgH2 powders would take more than 40 min for complete desorption. From these kinetics results, it is clear that, as stated before, Fe has a strong kinetic effect in the desorption when comparing with powders of commercial MgH_2.

The behaviors described above can be explained in the same way as previously done for the absorption, i.e., mainly the effects related to porosity (Fig. 2) and grain sizes (Table 1) and, of course, the catalytic effect of Fe that was present in all the samples. In this case, even though the differences between V1 and V5 were small, the speed of 1 mm/min was the best processing speed, since

no significant grain growth of Mg and Fe has occurred and the porosity was the largest compared to all of the extruded conditions studied.

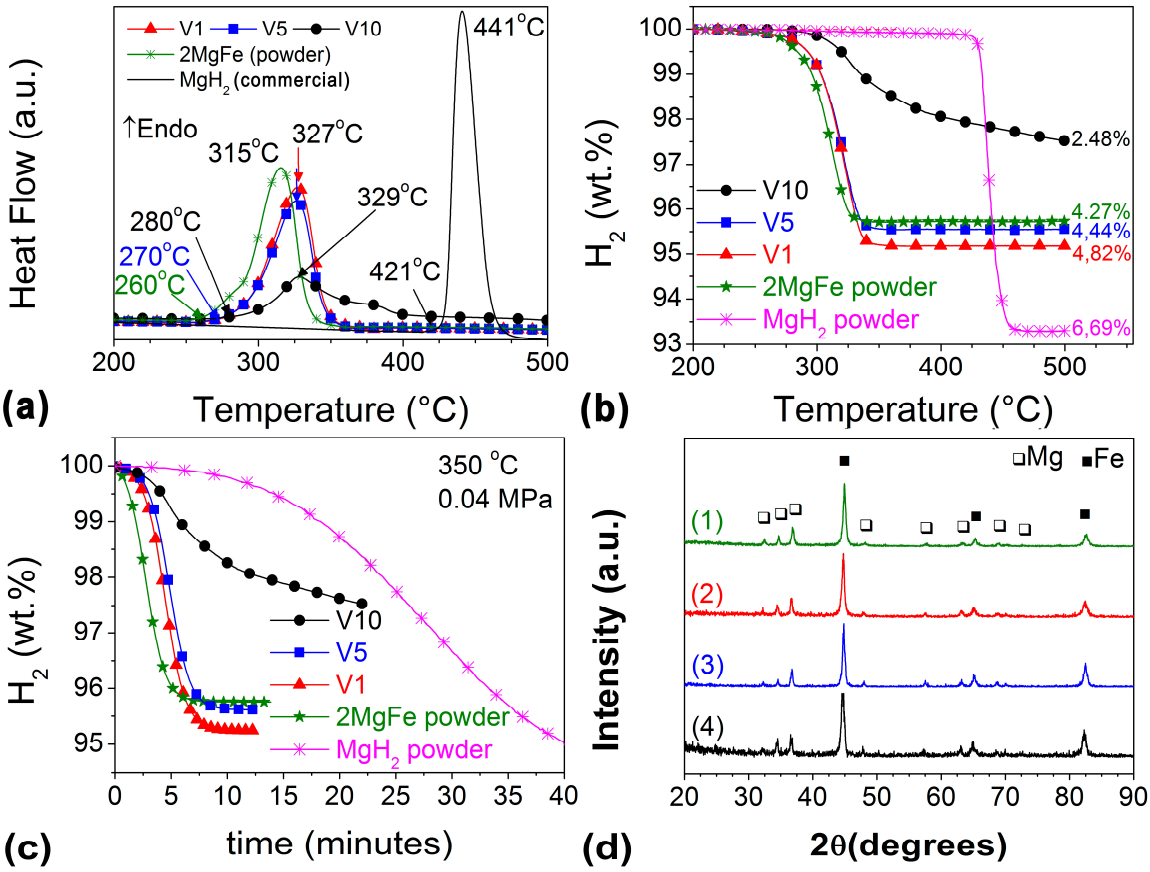

Figure 7 - Thermal analyzes of hydrogenated mixtures of 2Mg-Fe extruded under conditions V1, V5, and V10 (in comparison with powders of 2MgFe and commercial MgH2). (a) DSC. (b) TG. (c) Desorption kinetics at 350 °C under a pressure of 0.04 MPa of hydrogen for extruded samples compared to powders of 2MgFe and commercial MgH2. (d) XRD patterns for samples after desorption (a) powders of 2MgFe, (2) V1, (3) V5, and (4) V10.

Finally, but not less relevant, Figure 7d presents the XRD results of as-desorbed samples. By comparing these results it the ones from Figure 1, it will be

possible to observe that, after dehydrogenation, as expected, the samples return to their initial state, i.e., Mg and Fe are kept in the same ratio.

Summary

We have evaluated the changes in microstructure and the effect on hydrogen sorption behavior in 2Mg-Fe samples compacted by hot-extrusion using different ram speeds. The extrusion ram speed that produced samples with better hydrogenation properties was of 1 mm/min. The grain size increases and the porosity decreases with ram speed increasing, thus worsening the hydrogenation properties. Grain growth was not as expressive, remaining in the range of few nanometers, probably due to the pinning effect of nanometric Fe. During extrusion, Fe was redistributed along with consolidated samples but was kept agglomerated in the powders, thus decreasing powders capacity when compared with the best-extruded conditions. For all studied conditions, there was residual Fe, besides helping to pin grain boundaries during hydrogen absorption and desorption processes also help by acting as a catalyst in both cases. However, as expected, powders presented better absorption kinetics and saturated almost 5 hours before the sample extruded at 1mm/min (V1). During desorption, powders and bulks extruded at 1 (V1) and 5 (V5) mm/min presented the same kinetics and similar desorption temperatures, which were about 150 ^{o}C smaller than for powders of MgH_2. Samples with good absorption properties fully desorbed in less than 8 min at 350 ^{o}C, while commercial MgH2 would take much more than 40 min for complete desorption.

Acknowledgments

The authors would like to thank FAPESP (2014/21237-1) and CNPq (Universal 460471/2014-7) for financial support. AMJJ would like to acknowledge the CNPq (Brazil) under grant #301429/2017-0. KRC would like to acknowledge the FAPESP (Brazil) under grant # 18/09548-2

References

[1] Sakintuna B, Lamari-Darkrim L, Hirscher H, Metal hydride materials for solid hydrogen storage. A review. Int. J. Hyd. Energy. 2007;32:1121-40.

[2] Schulz R, Huot J, Liang G, Boily S, Lalande G, Denis MC, et al. Recent developments in the applications of nanocrystalline materials to hydrogen Technologies, Mat. Sci. Eng. A. 1999;267:240-5.

[3] Shao H, He L, Lin H, Li HW. Progress and Trends in Magnesium-Based Materials for Energy-Storage Research: A Review. Energy Technol. 2018;6:445-8

[4] Zaluski L, Zaluska A, Strom-Olsen JO, Nanocrystalline metal hydrides, J. Alloys Compd. 1997;253-254:70-9.

[5] Zaluska, Zaluski L, Strom-Olsen JO, Nanocrystalline magnesium for hydrogen storage, J. Alloys Compd. 1999;288:217-25.

[6] Castro JFR, Yavari AR, Lemoulec A, Ishikawa TT, Botta WJ. Improving H-sorption in MgH2 powders by addition of nanoparticles of transition metal

fluoride catalysts and mechanical alloying, J. Alloys Compd. 2005;389:270-4.

[7] Leiva DR, Floriano R, Huot J, Jorge AM, Bolfarini C, Kiminami CS, et al. Nanostructured MgH2 prepared by cold rolling and cold forging. J. Alloys Comp. 2011;509:S444-8.

[8] Floriano R, Leiva DR, Deledda S, Hauback BC, Botta WJ. Nanostructured MgH2 Obtained by Cold Rolling Combined with Short-time High-energy Ball Milling. Mat. Res. 2013;16:158-67.

[9] Floriano R, Leiva DR, Deledda S, Hauback BC, Botta WJ. Cold rolling of MgH2 powders containing different additives. Int. J. Hyd. Energy. 2013;38:16193-8.

[10] Floriano R, Leiva DR, Deledda S, Hauback BC, Botta WJ. MgH2-based nanocomposites prepared by short-time high energy ball milling followed by cold rolling: A new processing route. Int. J. Hyd. Energy. 2014;39:4404-13.

[11] de Lima GF, Leiva DR, Ishikawa TT, Bolfarini C, Kiminami CS, Botta WJ, Jorge Jr AM. Hydrogen Sorption Properties of the Complex Hydride Mg2FeH6 Consolidated by HPT. Mat. Sci. Forum. 2010;667-669:1053-8.

[12] Løken S, Solberg JK, Maehlen JP, Denys RV, Lototsky MV, Tarasov BP et al. J. Alloys Compd. 2007;446-447:114. J. Alloys Compd. 2007;446-447:114-20.

[13] Skripnyuk VM, Buchman E, Rabkin E, Estrin Y, Popov M, Jorgensen S. The effect of equal channel angular pressing on hydrogen storage properties of a eutectic Mg–Ni alloy. J. Alloys Compd. 2007;436:99-106.

[14] Skripnyuk VM, Rabkin E, Estrin Y, Lapovok R. The effect of ball milling and equal channel angular pressing on the hydrogen absorption/desorption

properties of Mg–4.95 wt% Zn–0.71 wt% Zr (ZK60) alloy. Acta Mater. 2004; 52:405–14.

[15] Leiva DR, Costa HCA, Huot J, Pinheiro T S, Jorge Jr AM, Ishikawa TT, Botta WJ. Magnesium-Nickel Alloy for Hydrogen Storage Produced by Melt Spinning Followed by Cold Rolling. Mat. Res. 2012;15:813-7.

[16] Soyama J, Triques MRM, Leiva DR, Jorge Jr AM, da Silva EP, Pinto HC, et al. Hydrogen storage in heavily deformed ZK60 alloy modified with 2.5 wt.% Mm addition. Int. J. Hyd. Energy. 2016;41:4177-84.

[17] Lima GF, Triques MRM, Kiminami CS, Botta WJ, Jorge Jr. AM. Hydrogen storage properties of 2Mg–Fe after the combined processes of hot extrusion and cold rolling. J. Alloys Compd. 2014;586:S409–12.

[18] Lima-Andreani GF, Triques MRM, Kiminami CS, Botta WJ, Roche V, Jorge Jr. AM. Characterization of hydrogen storage properties of Mg-Fe-CNT composites prepared by ball milling, hot-extrusion and severe plastic deformation methods. Int. J. Hyd. Energy. 2016;41:23092-8.

[19] Antiqueira FJ, Leiva, Ishikawa TT, Jorge Jr., Botta WJ. Severe Plastic Deformation and Additive Distribution in Mg-Fe to Improve Hydrogen Storage Properties. Mat. Res. 2017;20:61-70.

[20] Popilevsky L, Skripnyuk VM, Estrin Y, Dahle A, Gattia DM, Montone A, et al. Hydrogenation-induced microstructure evolution in as cast and severely deformed Mg-10 wt.% Ni alloy. Int. J. Hyd. Energy. 2013;38:12103-14.

[21] Hongo T, Edalati K, Arita M, Matsuda J, Akiba E, Horita Z. Significance of grain boundaries and stacking faults on hydrogen storage properties of Mg2Ni intermetallics processed by high-pressure torsion. Acta Mater. 2015;92:46-54.

[22] Edalati K, Emami H, Staykov A, Smith DJ, Akiba E, Horita Z. Formation of metastable phases in magnesium–titanium system by high-pressure torsion and their hydrogen storage performance. Acta Mater. 2015;99:150-6.

[23] Edalati K, Emami H, Ikeda Y, Iwaoka H, Tanaka I, Akiba E, Horita Z. New nanostructured phases with reversible hydrogen storage capability in immiscible magnesium–zirconium system produced by high-pressure torsion. Acta Mater. 2016;108:293-303

[24] Márquez J, Leiva DR, Floriano R, Silva WB, Ishikawa TT, Kiminami CS, Botta WJ. Hydrogen storage in MgH2LaNi5 composites prepared by cold rolling under inert atmosphere. Int. J. Hyd. Energy. 2018;43:13348-55.

[25] Alsabawi K, Gray EM, Webb CJ. The effect of ball-milling gas environment on the sorption kinetics of MgH2 with/without additives for hydrogen storage. Int. J. Hyd. Energy. 2019;44:2976-80.

[26] Tian M, Shang C. Mg-based composites for enhanced hydrogen storage performance. Int. J. Hyd. Energy. 2019;44: 338-44.

[27] Yahya MS, Sulaiman NN, Mustafa NS, Yap FAH, Ismail M. Improvement of hydrogen storage properties in MgH2 catalysed by K2NbF7. Int. J. Hyd. Energy. 2018;43:14532-40.

[28] Thongtan P, Dansirima P, Thiangviriya S, Thaweelap N, Suthummapiwat A, Plerdsranoy P, Utke R. Reversible hydrogen sorption and kinetics of hydrogen storage tank based on MgH2 modified by TiF4 and activated carbon. Int. J. Hyd. Energy. 3018;43: 12260-70.

[29] Youn J-S, Phan D-T, Park C-M, Jeon K-J. Enhancement of hydrogen sorption properties of MgH2 with a MgF2 catalyst. Int. J. Hyd. Energy. 2017;42: 20120-4.

[30] Alsabawi K, Webb TA, Gray EM, Webb CJ. Kinetic enhancement of the sorption properties of MgH2 with the additive titanium isopropoxide. International Int. J. Hyd. Energy. 2017;42:5227-34.

[31] Kumar S, Jain U, Jain A, Miyaoka H, Ichikawa T, Kojima Y, Dey GK. Development of MgLiB based advanced material for onboard hydrogen storage solution. Int. J. Hyd. Energy. 2017;42:3963-70.

[32] Yavari AR, Lemoulec A, Castro JFR, Deledda S, Friedrichs O, Botta WJ, Vaughan G, Klassen T, Fernandez A, Kvick A. Improvement in H-sorption kinetics of MgH2 powders by using Fe nanoparticles generated by reactive FeF3 addition, Scri. Mater. 2005;52:719-24.

[33] Bogdanovic B, Reiser A, Schlichte K, Spliethoff B, Tesche B. Thermodynamics and dynamics of the Mg–Fe–H system and its potential for thermochemical thermal energy storage, J. Alloys Compd. 2002;345:77-89.

[34] Huot J, Boily S, Akiba E, Schulz R. Direct synthesis of Mg2FeH6 by mechanical alloying, J. Alloys Compd. 1998;280:306-9.

[35] Gennari FC, Castro FJ, Gamboa A. Synthesis of Mg2FeH6 by reactive mechanical alloying: formation and decomposition properties. J. Alloys Compd. 2002;339:261-7.

[36] Li S, Varin RA, Morozova O, Khomenko T. Controlled mechano-chemical synthesis of nanostructured ternary, J. Alloys Compd. 2004;384:231-48.

[37] Raman SSS, Davidson DJ, Bobet JL, Srivastava ON. Investigations on the synthesis, structural and microstructural characterization of Mg-based K2PtCl6 type (Mg2FeH6) hydrogen storage material prepared by mechanical alloying, J. Alloys Compd. 2002;333:282-90.

[38] Huot J, Hayakawa H, Akiba E. Preparation of the hydrides Mg2FeH6 and Mg2CoH5 by mechanical alloying followed by sintering, J. Alloys Compd. 1997;248:164-7.

[39] Castro FJ, Gennari FC. Effect of the nature of the starting materials on the formation of Mg2FeH6, J. Alloys Compd. 2004;375:292-6.

[40] Herrich M, Ismail N, Lyubina J, Handstein A, Pratt A, Gutfleisch O. Synthesis and decomposition of Mg2FeH6 prepared by reactive milling. Mat. Sci. Eng. B. 2004;108:28-32.

[41] Ueda TT, Tsukahara M, Kamiya Y, Kikuchi S. Preparation and hydrogen storage properties of Mg–Ni–Mg2Ni laminate composites, J. Alloys Compd. 2005;386:253-7.

[42] Dufour J, Huot J. Rapid activation, enhanced hydrogen sorption kinetics and air resistance in laminated Mg–Pd 2. 5 at. %, J. Alloys Compd. 2007;439: L5-L7.

[43] Dufour J, Huot J. Study of Mg6Pd alloy synthesized by cold rolling, J. Alloys Compd. 2007;446–447:147–51.

[44] Takeichi N, Tanaka K, Tanaka H, Ueda TT, Kamiya Y, Tsukahara M, Miyamura H, Kikuchi S. Hydrogen storage properties of Mg/Cu and Mg/Pd laminate composites and metallographic structure, J. Alloys Compd. 2007;446–447:543–48.

[45] Leiva DR, Fruchart D, Bacia M, Girard G, Skriabina N, Villela ACS, Miraglia S, Santos DS, Botta WJ. Mg alloy for hydrogen storage processed by SPD, Int. J. Mat. Res. 2009;100:1-8.

[46] Kusadome Y, Ikeda K, Nakamori Y, Orimo S, Horita Z. Hydrogen storage capability of MgNi2 processed by high-pressure torsion, Scri. Mater. 2007;57:751-3.

[47] Lima GF, Peres MM, Garroni S, Baró MD, Surinyach S, Kiminami CS, Ishikawa TT, Botta WJ, Jorge Jr AM. Microstructural characterization, and hydrogenation study of extruded MgFe alloy, J. Alloys Compd. 2010;504:S299–S301.

[48] Lima GF, Garroni S, Baró MD, Surinyach S, Kiminami CS, Botta WJ, Peres MM, Jorge Jr AM. 2Mg–Fe alloys processed by hot-extrusion. Influence of processing temperature and the presence of MgO and MgH2 on hydrogenation sorption properties, J. Alloys Compd. 2011;509S:S460–3

[49] Cerutti R, Lima GF, Kiminami CS, Botta WJ, Jorge Jr AM. 2Mg–Fe and 2Mg–Fe+5%C mixtures processed by hot extrusion. Influence of carbon on hydrogen sorption properties, J. Alloys Compd. 2011;509S:S464-7

[50] de Lima GF, Garroni S, Baró MD, Suriñach S, Kiminami CS, Botta WJ, Jorge Jr AM. Hydrogen storage properties of 2Mg-Fe mixtures processed by hot extrusion. Influence of the extrusion ratio. Int J Hyd. Energy 2012; 37:15196-203.

[51] Jorge Jr AM, de Lima GF, Triques MRM, Botta WJ, Kiminami CS, Nogueira RP, Yavari AR, Langdon TG. Correlation between hydrogen storage properties and texture induced in magnesium through ECAP and cold rolling. Int J Hyd. Energy 2014; 39:3810-21.

[52] de Lima-Andreani GF, Miglioli MM, Triques MRM, Roche V, Kiminami CS, Botta WJ, Jorge Jr AM. Hydrogen storage properties of 2Mg-Fe mixtures

processed by hot extrusion at different temperatures. Int J Hyd. Energy 2017; 42:11493-500.

[53] Asselli AAC, Leiva DR, Cozentino GH, Floriano R, Huot J, Ishikawa TT, Botta WJ. Hydrogen storage properties of MgH2processed by cold forging. J. Alloys Comp. 2014;615S:S719-24.

[54] Panda S, Fundenberger J-J, Zhao Y, Zou J, Toth LS, Grosdidier T. Effect of initial powder type on the hydrogen storage properties of high-pressure torsion consolidated Mg. Int. J. Hyd. Energy. 2017;42:22438-48.

[55] Panda S, Toth LS, Zou J, Grosdidier T. Effect of Strain Heterogeneities on Microstructure, Texture, Hardness, and H-Activation of High-Pressure Torsion Mg Consolidated from Different Powders. Materials. 2018;11:1335-54.

[56] Márquez JJ, Soyama J, Silva RA, Leiva DR, Floriano R, Ishikawa TT, Kiminami CS, Botta WJ. Processing of MgH2 by extensive cold rolling under protective atmosphere. Int. J. Hyd. Energy. 2017;42:2201-8.

[57] Edalati K, Kitabayashi K, Ikeda Y, Matsuda J, Li H-W, Tanaka I, Akiba E, Horita Z. Bulk nanocrystalline gamma magnesium hydride with low dehydrogenation temperature stabilized by plastic straining via high-pressure torsion. Scripta Mater. 2018;157:54-7.

[58] Revesz A, Gajdics M, Schafler E, Calizzi M, Pasquini L. Dehydrogenation-hydrogenation characteristics of nanocrystalline Mg2Ni powders compacted by high-pressure torsion. J. Alloys Compd. 2017;702:84-91.

[59] Jorge Jr AM, Prokofiev E, de Lima GF, Rauch E, Veron M, Botta WJ, Kawasaki M, Langdon TG. An investigation of hydrogen storage in a

magnesium-based alloy processed by equal-channel angular pressing. Int. J. Hyd. Energy. 2013;38:8306-12.

[60] Révész Á, Gajdics M, Varga L, Krállics G, Péter L, Spassov T. Hydrogen storage of nanocrystalline Mg–Ni alloy processed by equal-channel angular pressing and cold rolling. Int. J. Hyd. Energy. 2014;39:9911-17.

[61] Zou JX, Pérez-Brokate CF, Arruffat R, Bolle B, Fundenberger JJ, Zeng XQ, Grosdidier T, Ding WJ. Nanostructured bulk Mg + MgO composite synthesized through arc plasma evaporation and high pressure torsion for H-storage application. Mater. Sci. Eng. B. 2014;183:1-5.

[62] Asselli AAC, Leiva DR, Huot J, Kawasaki M, Langdon TG, Botta WJ. Effects of equal-channel angular pressing and accumulative roll-bonding on hydrogen storage properties of a commercial ZK60 magnesium alloy. Int. J. Hyd. Energy. 2015;40:16971-6.

[63] Grosdidier T, Fundenberger JJ, Zou JX, Pan YC, Zeng XQ. Nanostructured Mg based hydrogen storage bulk materials prepared by high pressure torsion consolidation of arc plasma evaporated ultrafine powders. Int. J. Hyd. Energy. 2015;40:16985-991.

[64] Grill A, Horky J, Panigrahi A, Krexner G, Zehetbauer M. Long-term hydrogen storage in Mg and ZK60 after Severe Plastic Deformation. Int. J. Hyd. Energy. 2015;40:17144-52.

[65] Faisal M, Gupta A, Shervani S, Balani K, Subramaniam A. Enhanced hydrogen storage in accumulative roll bonded Mg-based hybrid. Int. J. Hyd. Energy. 2015;40:11498-505.

[66] Wang L, Jiang J, Ma A, Li Y, Song D. Metals. A Critical Review of Mg-Based Hydrogen Storage Materials Processed by Equal Channel Angular Pressing. Metals. 2017;7:324-36.

[67] Leiva DR, Chanchetti F, Floriano R, Ishikawa TT, Botta WJ. Exploring several different routes to produce Mg-based nanomaterials for Hydrogen storage. IOP Conf. Series. Mater. Sci. Eng. 2014;63:012115.

[68] Botta WJ, Jorge Jr AM, Veron M, Rauch EF, Ferrie E, Yavari AR, Huot J, Leiva DR. H-sorption properties and structural evolution of Mg processed by severe plastic deformation. J. Alloys Comp. 2013;580S:S187-91.

[69] Floriano R, Leiva DR, Carvalho JA, Ishikawa TT, Botta WJ. Cold rolling under inert atmosphere: A powerful tool for Mg activation. Int. J. Hyd. Energy. 2014;39:4959-65.

[70] Lima GF, Triques MRM, Kiminami CS, Botta WJ, Jorge Jr AM. Hydrogen storage properties of pure Mg after the combined processes of ECAP and cold-rolling. J. Alloys Compd. 2014;586:S405–8.

[71] Jorge Jr AM, Prokofiev E, Triques MRM, Roche V, Botta WJ, Kiminami CS, Raab GI, Valiev RZ, Langdon TG. Effect of cold rolling on the structure and hydrogen properties of AZ91 and AM60D magnesium alloys processed by ECAP. Int. J. Hyd. Energy. 2017;42:21822-31.

[72] Soyama J, Triques MRM, Leiva DR, Jorge Jr AM, da Silva EP, Pinto HC, Bolfarini C, Kiminami CS, Botta WJ. Severely deformed ZK60 + 2.5% Mm alloy for hydrogen storage produced by two different processing routes. Int. J. Hyd. Energy. 2016;41:11284-92.

[73] Floriano R, Leiva DR, Melo GC, Huot J, Kaufman M, Figueroa S, Mendoza-Zélis LA, Damonte LC, Botta WJ. Low temperature rolling of AZ91 alloy for hydrogen storage. Int. J. Hyd. Energy. 2017;42:29394-405.

[74] Lima GF, Jorge Jr AM, Leiva DR, Kiminami CS, Bolfarini C, Botta WJ. Severe plastic deformation of Mg-Fe powders to produce bulk hydrides. J. Phys. Conf. Series. 2009;144:012015.

[75] Edalati K, Uehiro R, Ikeda Y, Lia H-W, Emami H, Filinchuk Y, Arita M, Sauvage X, Tanaka I, Akiba E, Horita Z. Design and synthesis of a magnesium alloy for room temperature hydrogen storage. Acta Mater. 2018;149:88-96.

[76] Varin RA, Czujko T, Wronski ZS. Nanomaterials for Solid State Hydrogen Storage. New York: Springer, 2009, pg 58, and 65 to 67]

[77] Lutterotti L, Ceccato R, DalMaschio R, Pagani E. Quantitative Analysis of Silicate Glass in Ceramic Materials by the Rietveld Method. Mater Sci Forum. 1998;87:278-81.

[78] Lutterotti L. MAUD - Materials Analysis Using Diffraction, http://maud. radiographema.eu/;2019 [accessed February 2019].

[79] Pavlinov LV, Gladyshev AM, Bykov VN. Self-Diffusion in Calcium and Diffuse of Barely Soluble Impurities in Magnesium and Calcium. Phys. Met. Metallogr. 1968;26:53.

[80] Zhou B-C, Shang S-L, Wang Y, Liu Z-K. Diffusion coefficients of alloying elements in dilute Mg alloys: A comprehensive first-principles study. Acta Mater. 2016;103:573–86.

[81] Batalović K, Radaković J, Belošević-Čavor J, Koteski V. Transition metal doping of Mg2FeH6– a DFT insight into synthesis and electronic structure. Phys. Chem. Chem. Phys. 2014;16:12356.